Passive fathometer reflector identification with phase shift modeling

Zoi-Heleni Michalopoulou
Department of Mathematical Sciences, New Jersey Institute of Technology, Newark, New Jersey 07102, USA
michalop@njit.edu

Peter Gerstoft
Marine Physical Laboratory, Scripps Institution of Oceanography, La Jolla, California 92093-0238, USA
gerstoft@ucsd.edu

Abstract: In passive fathometer processing, the presence of wavelets in the estimate of the medium's Green's function corresponds to the location of reflectors in the seabed; amplitudes are related to seabed properties. Bayesian methods have been successful in identifying reflectors that define layer interfaces. Further work, however, revealed that phase shifts are occasionally present in the wavelets and hinder accurate layer identification for some reflectors. With a Gibbs sampler that computes probability densities of reflector depths, strengths of the reflections, and wavelet phase shifts, the significance of phase shift modeling in successful estimation of reflectors and their strengths is demonstrated.

[CFG]
Date Received: December 15, 2015 **Date Accepted:** May 10, 2016

1. Introduction

Passive fathometer data processing[1–10] is a coherent ambient noise processing technique that enables passive ocean bottom profiling. The fathometer output is the cross-correlation of downward traveling sea surface noise generated just above a vertical line array (VLA) with the upward traveling reflection of itself from the seabed. To achieve this, conventional or adaptive beamforming is used on the VLA data. Beamforming allows the array to look up and down while rejecting arrivals from other angles, particularly the higher level arrivals coming from around the horizontal direction (that is, due to regional shipping activity). We are here using standard conventional fathometer processing[1,3] to obtain the passive fathometer response as shown in Fig. 1, which illustrates the output for the Boundary 2003 experiment (first 100 records in Fig. 5 of Ref. 8, where adaptive processing was used). The strong reflector at about 133 m is below the seabed. The reflections above are due to weak reflectors and maybe to some ringing related to the processing.

Let the probing signal transmitted to the seabottom have bandwidth BW (3950 Hz, here) with uniform frequency amplitude and zero phase. It is only changing in phase as it propagates deeper. Assuming a simple layer interface, a frequency-independent reflection coefficient, and flat zero-phase spectra for upward and downward propagating noise, and also ignoring multiple reflections, each interface results in a $\mathrm{sinc}(t) = \sin(t)/t$ wavelet at the fathometer output, corresponding to its two-way travel time.[3] Assuming a sound speed c, the time-domain fathometer response at the two-way travel time t due to a reflector at a depth z_i (corresponding to two-way travel time $t_i = 2z_i/c$) is given by

$$s(t, z_i, a_i) = \mathrm{sinc}\left(2BW\left(t - \frac{2z_i}{c}\right)\right), \tag{1}$$

where the time-domain amplitude of the fathometer output is assumed to be unity; symbol a_i denotes the strength of the reflection, determined by the reflector properties. The fathometer output is available at sampling times corresponding to the acoustic data sampling frequency f_s.

While this model works reasonably in practice, there are several reasons why it might not be accurate. For example, the phase of the wavelet could vary across frequency, in addition to having a phase delay caused by the two-way travel time from the reflector. Also closely spaced reflectors can appear as a phase distorted wavelet. While the wavelet could be more complicated, in this work we search for sinc wavelets with a constant phase offset across the whole bandwidth. We associate each reflector with an unknown amplitude a_i and phase φ_i:

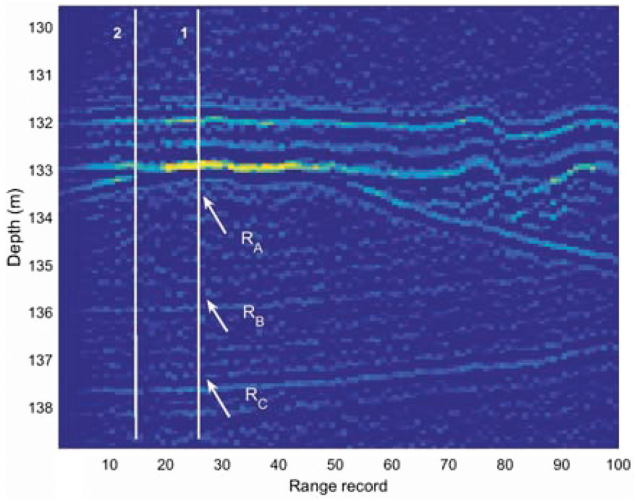

Fig. 1. (Color online) Fathometer output from the Boundary 2003 experiment. The two lines indicate traces that will be analyzed further.

$$s(t, z_i, \phi_i) = \mathrm{F}^{-1}(\mathrm{F}(s(t, z_i, a_i))e^{i\omega t}), \tag{2}$$

where F (and F^{-1}) represents the (inverse) Fourier transform. A phase distorted sinc function will be shown later.

The paper is organized as follows. Section 2 presents the method employed for the estimation of reflector depths and their associated strengths and phase shifts. Section 3 demonstrates the importance of phase modeling in both reflector depth and amplitude estimation. Conclusions follow in Sec. 4.

2. Gibbs sampling

Estimates of unknown parameters of a statistical model are obtained through the maximization of the posterior probability density functions (PDFs) of these parameters given the observed data and quantitatively described prior knowledge. Assuming a received reflection trace $r(d)$ consisting of M reflector responses and noise, we can write

$$r(d) = \sum_{i=1}^{M} a_i s(d - d_{z_i}, \phi_i) + w(d), \tag{3}$$

where $d = 1,\ldots,D$ (D is the number of depth samples). For the ith reflection, a_i, d_{z_i}, and φ_i are the amplitude, the sample corresponding to reflector location, and the phase shift, respectively. Noise $w(d)$ is assumed to be additive and white normally distributed with zero mean and variance σ^2. Most importantly, $s(d - d_{z_i}, \varphi_i)$ is the phase-shifted wavelet.

We want to estimate the PDFs for d_{z_i}, the depth samples corresponding to the locations of the reflectors, and a_i, the corresponding amplitudes, $i = 1,\ldots,M$. Within the process, we need to estimate phase shifts φ_i, as they affect the estimation of the other unknowns.

Variance σ^2 is also included as a nuisance parameter; setting variance as a known quantity can have destructive effects on the parameter estimates. The number of reflectors M is initially assumed to be known; this assumption will be relaxed later. We use the Gibbs Sampler of Ref. 11 with a significant change: now we have M additional unknowns, the phase shifts φ_i. Below we implement the process of Ref. 11, adapted to our problem.

Let $\mathbf{d} = [d_{z_1},\ldots,d_{z_M}]$, $\mathbf{a} = [a_1,\ldots,a_M]$, and $\varphi = [\varphi_1,\ldots,\varphi_M]$. For the Gibbs sampler, since the noise is $N(0, \sigma^2)$, the likelihood of the unknown parameters is found from Eq. (3):

$$l(\mathrm{d}, \mathrm{a}, \phi, \sigma^2 | r(d)) \propto \exp\left\{ -\frac{1}{2\sigma^2} \sum_{z=1}^{D} \left[r(d) - \sum_{i=1}^{M} a_i s(d - d_{z_i}, \phi_i) \right]^2 \right\}. \tag{4}$$

Next we select prior densities that, combined with the likelihood, will help in the construction of the posterior PDFs. Uniform priors are selected for the reflection amplitudes a_i, reflector depths d_{z_i}, and phase shifts φ_i,

$$p(a_i) = \frac{1}{2A}, \quad -A \le a_i A, \ i = 1, \ldots, M. \tag{5}$$

$$p(d_{z_i}) = \frac{1}{D}, \quad 1 \le d_{z_i} \le D, \ i = 1, \ldots, M, \tag{6}$$

$$p(\phi_i) = \frac{1}{\pi}. \tag{7}$$

The phase in $[0, \pi)$ along with the amplitude sign can represent phase shifts in $[\pi, 2\pi)$.

An improper uniform prior is selected for log σ^2, taking positive and negative values,[12]

$$p(\sigma^2) = 1/\sigma^2. \tag{8}$$

Multiplying priors and likelihood provides the PDF of all unknowns given the data $r(d)$:

$$p\left(\mathrm{d}, \mathrm{a}, \phi, \sigma^2 | r(d)\right) = C \exp\left\{-\frac{1}{2\sigma^2}\sum_{d=1}^{D}\left[r(d) - \sum_{i=1}^{M} a_i s(d - d_{z_i}, \phi_i)\right]^2\right\}. \tag{9}$$

The Gibbs sampler computes the joint posterior PDF of Eq. (9), which can be then used for the estimation of marginal PDFs as well as maximum *a posteriori* (MAP) estimates. For the implementation of this Monte Carlo method, we need the conditional posterior densities for all parameters. Some of the conditional densities are formulated analytically; others are calculated on a grid.

We first consider amplitudes a_j, $j = 1, \ldots, M$ and $j \neq i$, and delays d_{z_i}, $i = 1, \ldots, M$, to be known. With algebraic manipulations of Eq. (9) and using unit-norm wavelets $\Sigma_{d=1}^{D} s(d - d_{z_i}, \phi_i)^2 = 1$, we derive the following conditional density for amplitude a_i ($\tilde{a}$ is a without a_i):

$$p\left(a_i | \mathrm{d}, \tilde{a}, \phi, \sigma^2, r(d)\right) = C \exp\left(-\frac{1}{2\sigma^2}\left\{a_i - \sum_{d=1}^{D}\left[r(d)s(d - d_{z_i}, \phi_i) - \sum_{j=1(j\neq i)}^{M} a_j s(d - d_{z_i}, \phi_i) s\left(d - d_{z_i}, \phi_j\right)\right]\right\}^2\right). \tag{10}$$

From the exponential of Eq. (10), a Gaussian density for a_i is identified as

$$\mathcal{N}\left(a_i - \sum_{d=1}^{D}\left[r(d)s(d - d_{z_i}, \phi_i) - \sum_{(j\neq i)}^{M} a_j s(d - d_{z_i}, \phi_i) s(d - d_{z_j}, \phi_j)\right], \sigma^2\right).$$

This is expected because of the linear relationship between data and amplitudes in Eq. (3) and the Gaussian noise in the data. We draw samples for these parameters in a straightforward way.[11]

Similarly, for variance σ^2, considering prior and likelihood gives

$$p\left(\sigma^2 | \mathrm{d}, \mathrm{a}, \phi, r(d)\right) = Q \frac{1}{\sigma^{D+2}} \exp\left\{-\frac{1}{2\sigma^2}\sum_{d=1}^{D}\left[r(d) - \sum_{i=1}^{M} a_i s(d - d_{z_i}, \phi_i)\right]^2\right\}. \tag{11}$$

The density of Eq. (11) is an inverse χ^2 (Ref. 12) from which samples can be readily drawn.[11]

The marginal conditional posterior densities for depths d_{z_i}, $i = 1, \ldots, M$, are calculated on a grid. Using the density of Eq. (9), the conditional posterior density of d_{z_i} is ($\tilde{\mathbf{d}}$ is $\mathbf{d}$ without d_{z_i}),

$$p\left(d_{z_i} | \tilde{d}, \mathrm{a}, \phi, \sigma^2, r(d)\right) = G \exp\left\{-\frac{1}{2\sigma^2}\sum_{z=1}^{D}\left[r(d) - \sum_{i=1}^{M} a_i s(d - d_{z_i}, \phi_i)\right]^2\right\}. \tag{12}$$

The grid is divided in D candidate depths for the reflector positions. The conditional PDFs of phase shifts are also defined on a grid ($\tilde{\varphi}$ is φ without φ_i),

$$p\left(\phi_i | \mathrm{d}, \mathrm{a}, \tilde{\phi}, \sigma^2, r(d)\right) = K \exp\left\{-\frac{1}{2\sigma^2}\sum_{d=1}^{D}\left[r(d) - \sum_{i=1}^{M} a_i s(d - d_{z_i}, \phi_i)\right]^2\right\}. \tag{13}$$

Initial conditions are selected for all unknowns: d_{z_i}, a_i, φ_i, and σ. Then, conditional on all those values, a sample for one of the parameters is drawn, reflecting its

current state. The process is repeated for all other parameters. After updating all of them, the process proceeds with the next iteration. We first update the amplitudes and then continue with variance, reflector depths, and phase shifts. Once initial iterations necessary for convergence are completed, the samples drawn for the remaining iterations represent the joint PDF of all parameters. The model order (number of reflectors M) is estimated using the Schwarz-Rissanen criterion[13] by running the Gibbs sampler for different values of M and calculating function f in Eq. (14),

$$f(M) = 2\left(\frac{D}{2}+1\right)\log\hat{\sigma} + \frac{1}{2\hat{\sigma}^2}\sum_{z=1}^{D}\left[r(d) - \sum_{i=1}^{M}\hat{a}_i s\left(d-\hat{d}_{z_i},\hat{\phi}_i\right)\right]^2 + M\log D. \quad (14)$$

Function f is computed for $M_2 - M_1 + 2$ runs of the Gibbs sampler for values of M between M_1 and M_2.

Here, we select $M_1 = 9$ and $M_2 = 14$.

In Ref. 10 we found a maximum of nine reflectors. However, the method in this work, handling data that have not been smoothed, provides higher resolution and identifies more layers. Symbols $\hat{d}_{z_i}$, $\hat{a}_i$, and $\hat{\varphi}_i$ correspond to the MAP estimates of depths, amplitudes, and phase shifts for the M arrivals; $\hat{\sigma}$ is the MAP estimate of standard deviation. The value M minimizing function f is the model order. This process is equivalent to maximizing the posterior PDF of M, conditional on the MAP estimates of the other parameters. For depth and amplitude estimation under the zero-phase assumption, the same process was followed after setting $\varphi_i = 0$, $i = 1,\ldots,M$.

3. Estimation with phase shift modeling

We consider "slices" showing depth series at distinct range records from the fathometer response of Fig. 1. Figure 2 shows the depth reflection series when (a) we estimate wavelet phase shifts and (b) we consider all wavelets to have zero-phase for the trace indicated by line 1 in Fig. 1; for the latter case, instead of Eq. (3), we use

$$r(d) = \sum_{i=1}^{M} a_i s(d - d_{z_i}) + w(d).$$

Symbols A_{ph}, B_{ph}, and C_{ph} correspond to arrivals identified by the Gibbs sampler with phase shift estimation. The respective reflectors are indicated with arrows in Fig. 1.

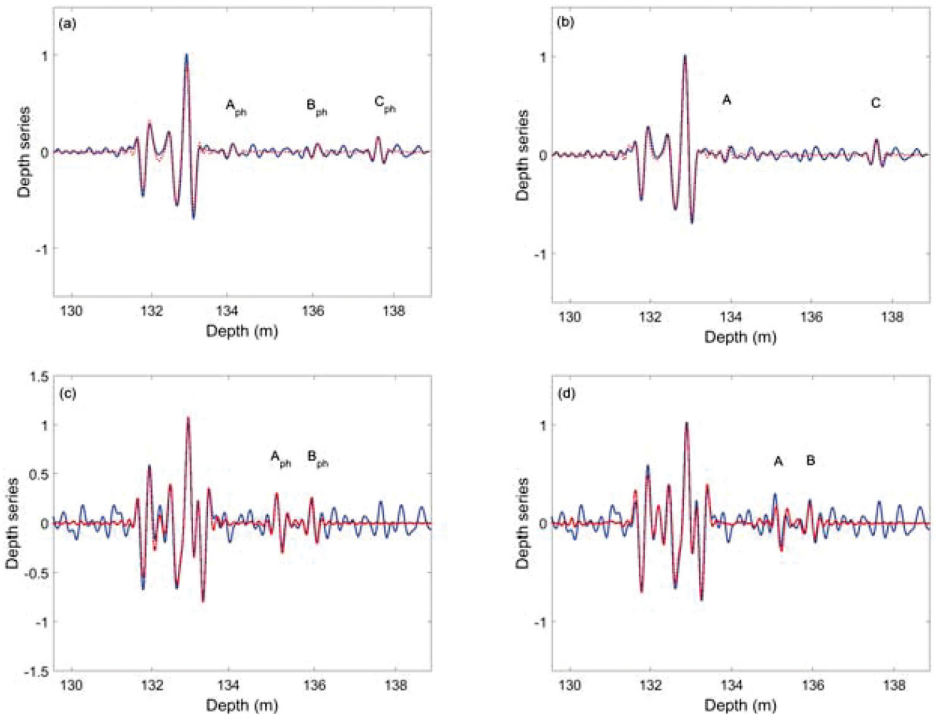

Fig. 2. (Color online) The depth reflection series for slices 1 [(a) and (b)] and 2 [(c) and (d)] in Fig. 1: (a) and (c) phase-shift modeling and (b) and (d) zero-phase wavelets. The depth-series are denoted by solid lines and the synthetic depth-series generated with the MAP estimates from the Gibbs Sampler are represented by dotted lines.

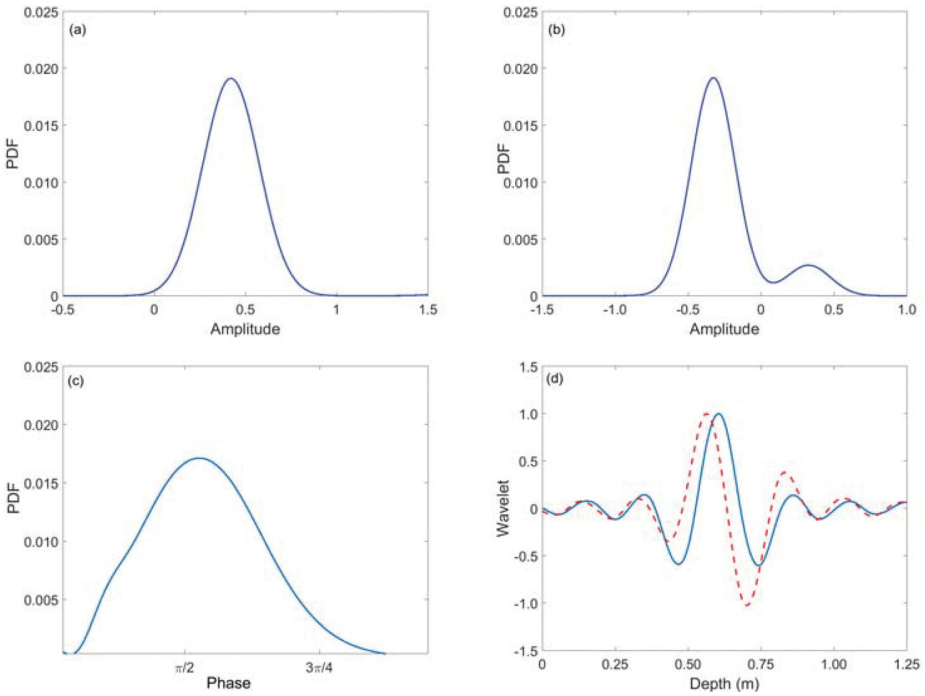

Fig. 3. (Color online) PDFs of amplitudes for arrivals (a) A_{ph} and (b) A. (c) The PDF of the phase shift for arrival A_{ph}. (d) The normalized waveform for arrival A_{ph} (dashed line) superimposed on a sinc pulse (solid line).

Symbols A and C show corresponding arrivals when phase shift is not considered. In the latter case, there is no arrival identified near 136 m. This is attributed to the lack of phase shift estimation: a good match between a sinc and the true arrival cannot be found. Although an arrival near 134 m is found, the match there is not as good as the match between the estimated and true depth-series when phase shift is inverted for [arrivals A and A_{ph} in Figs. 2(a) and 2(b), respectively].

Figures 2(c) and 2(d) show the depth-series when we estimate wavelet phase shifts and we consider all wavelets to have zero-phase for the trace indicated by line 2 in Fig. 1, respectively. Here, the two processors (with phase modeling or not) identify the same arrivals. However, the match of the true and estimated depth-series at A in Fig. 2(d) is poor. Looking more closely at the arrival, we see that the sinc there is inverted, which means that the amplitude is negative. Indeed, this is illustrated by the PDF of the amplitude for that arrival shown in Fig. 3(b), which is calculated with kernel density estimation;[14] the MAP estimate is −0.3. Figure 3(a) shows the PDF of the amplitude for arrival A_{ph} in Fig. 2(c). The PDF is maximized at 0.45. When no phase shift is considered, amplitudes can be poorly estimated. This is a significant problem, because amplitudes provide information on the physics of the sediments.

Figure 3(c) shows the PDF of the phase shift for A_{ph}. We then extract the phase corresponding to the MAP estimate from the PDF of Fig. 3(c). A plain sinc function (solid line) and the phase delayed sinc corresponding to the MAP estimate (dashed line) are shown in Fig. 3(d). When optimizing for layer reflections at event A, this has a marked influence in the waveform match.

4. Conclusions

The output of the fathometer is a depth-series of the subbottom response, which is modeled as a reflection response convolved with a sinc function. For each reflector we invert for depth, amplitude, and phase using a Gibbs Sampler, with the number of reflectors determined via the Schwarz-Rissanen criterion. The proposed algorithm is demonstrated on several traces from the Boundary 2003 experiment. We find that including the unknown phase in the estimation improves the data fit and, thus, reflector location and strength identification. Future processing will treat each reflector sequentially passing information from one reflector to the next using wavelets of uncertain phase.[10,15]

Acknowledgments

This work was supported by the Office of Naval Research through Grant Nos. N00014-13-1-0077, N00014-16-1-2485, and N00014-11-1-0439.

References and links

[1]M. Siderius, C. H. Harrison, and M. B. Porter, "A passive fathometer technique for imaging seabed layering using ambient noise," J. Acoust. Soc. Am. **120**(3), 1315–1323 (2006).

[2]C. H. Harrison and M. Siderius, "Bottom profiling by correlating beam-steered noise sequences," J. Acoust. Soc. Am. **123**(3), 1282–1296 (2008).

[3]P. Gerstoft, W. S. Hodgkiss, M. Siderius, C.-F. Huang, and C. H. Harrison, "Passive fathometer processing," J. Acoust. Soc. Am. **123**, 1297–1305 (2008).

[4]C. H. Harrison, "Anomalous signed passive fathometer impulse response when using adaptive beam forming," J. Acoust. Soc. Am. **125**(6), 3511–3513 (2009).

[5]J. Traer, P. Gerstoft, H. C. Song, and W. S. Hodgkiss, "On the sign of the adaptive passive fathometer impulse response," J. Acoust. Soc. Am. **126**(4), 1657–1658 (2009).

[6]M. Siderius, H. Song, P. Gerstoft, W. S. Hodgkiss, P. Hursky, and C. Harrison, "Adaptive passive fathometer processing," J. Acoust. Soc. Am. **127**(4), 2193–2200 (2010).

[7]J. Gebbie, M. Siderius, L. Muzi, and J. Paddock, "Extracting the Rayleigh reflection coefficient from the passive fathometer," in *OCEANS 2010*, September 2010, pp. 1–10.

[8]J. Traer, P. Gerstoft, and W. S. Hodgkiss, "Ocean bottom profiling with ambient noise: A model for the passive fathometer," J. Acoust. Soc. Am. **129**(4), 1825–1836 (2011).

[9]C. Yardim, P. Gerstoft, W. S. Hodgkiss, and J. Traer, "Compressive geoacoustic inversion using ambient noise," J. Acoust. Soc. Am. **135**(3), 1245–1255 (2014).

[10]Z.-H. Michalopoulou, C. Yardim, and P. Gerstoft, "Particle filtering for passive fathometer tracking," J. Acoust. Soc. Am. **131**(1), EL74–EL80 (2012).

[11]Z.-H. Michalopoulou and M. Picarelli, "Gibbs sampling for time-delay-and amplitude estimation in underwater acoustics," J. Acoust. Soc. Am. **117**(2), 799–808 (2005).

[12]G. Box and G. Tiao, *Bayesian Inference in Statistical Analysis* (Wiley, New York, 1992), pp. 1–585.

[13]M. Wax and T. Kailath, "Detection of signals by information theoretic criteria," IEEE Trans. Acoust. Speech Sign. Process. **33**(2), 387–392 (1985).

[14]A. E. Gelfand and A. F. M. Smith, "Sampling-based approaches to calculating marginal densities," J. Am. Stat. Assoc. **85**(410), 398–409 (1990).

[15]C. Yardim, Z.-H. Michalopoulou, and P. Gerstoft, "An overview of sequential Bayesian filtering in ocean acoustics," IEEE J. Ocean. Eng. **36**(1), 71–89 (2011).